



Published as: *Structure*. 2012 June 6; 20(6): 957–966.

## Improving the accuracy of macromolecular structure refinement at 7 Å resolution

Axel T. Brunger<sup>1</sup>, Paul D. Adams<sup>2</sup>, Petra Fromme<sup>3</sup>, Raimund Fromme<sup>3</sup>, Michael Levitt<sup>4</sup>, and Gunnar F. Schröder<sup>5</sup>

<sup>1</sup>Howard Hughes Medical Institute and Department of Molecular and Cellular Physiology, Stanford University School of Medicine, J.H. Clark Center, 318 Campus Drive, California 94305, USA

<sup>2</sup>Lawrence Berkeley National Laboratory, One Cyclotron Road, Bldg 64R0121, Berkeley, California 94720, USA

<sup>3</sup>Department of Chemistry and Biochemistry, Arizona State University, Tempe, Arizona 85287-1604, USA

<sup>4</sup>Department of Structural Biology, Stanford University School of Medicine, J.H. Clark Center, 318 Campus Drive, California 94305, USA

<sup>5</sup>Institute of Complex Systems (ICS-6), Forschungszentrum Jülich, 52425 Jülich, Germany

### SUMMARY

In X-ray crystallography, molecular replacement and subsequent refinement is challenging at low resolution. We compared refinement methods using synchrotron diffraction data of photosystem I at 7.4 Å resolution, starting from different initial models with increasing deviations from the known high-resolution structure. Standard refinement spoiled the initial models moving them further away from the true structure and leading to high  $R_{\text{free}}$ -values. In contrast, DEN-refinement improved even the most distant starting model as judged by  $R_{\text{free}}$ , atomic root-mean-square differences to the true structure, significance of features not included in the initial model, and connectivity of electron density. The best protocol was DEN-refinement with initial segmented rigid-body refinement. For the most distant initial model, the fraction of atoms within 2 Å of the true structure improved from 24% to 60%. We also found a significant correlation between  $R_{\text{free}}$ -values and the accuracy of the model, suggesting that  $R_{\text{free}}$  is useful even at low resolution.

### Keywords

DEN refinement; membrane protein; low-resolution refinement; simulated annealing; free  $R$  value

### INTRODUCTION

While increasingly complex macromolecules or assemblies have been successfully crystallized, such crystals often diffract weakly due to limited crystal growth, high crystal mosaicity or high sensitivity to radiation damage. Underlying causes can be inherent

© 2012 Elsevier Inc. All rights reserved.

Correspondence should be addressed to A.T.B (phone: 650-736-1031, fax: 650-745-1463, brunger@stanford.edu).

**Publisher's Disclaimer:** This is a PDF file of an unedited manuscript that has been accepted for publication. As a service to our customers we are providing this early version of the manuscript. The manuscript will undergo copyediting, typesetting, and review of the resulting proof before it is published in its final citable form. Please note that during the production process errors may be discovered which could affect the content, and all legal disclaimers that apply to the journal pertain.

flexibility, inhomogeneity, or disordered solvent components that prove difficult to overcome. Nevertheless, the interpretation of low-resolution diffraction is often desirable as it provides information about the interaction of individual components in the system or insights about large-scale conformational changes between different states of the system. In addition, macromolecular data collection continues to evolve, notably with microdiffraction synchrotron facilities (Sanishvili et al., 2008) and hard X-ray free electron lasers (FEL) (Chapman et al., 2011).

It is a well-known principle in crystallography that the accuracy of determined atomic positions exceeds the resolution limit of the diffraction data. At atomic resolution (around 1.2 Å), this arises from the excluded volumes of atoms: electron cloud repulsion keeps the scattering objects further apart than half the wavelength of the X-ray radiation used (1 to 2 Å resolution) allowing the centroids of the atomic electron density to be typically determined to better than 0.1 Å accuracy. At moderate resolution (up to about 4 Å), knowledge of the stereochemistry of the system (bond lengths, bond angles, fixed torsion angles, chirality) allows this principle to be applied to the majority of macromolecular crystal structures. At even lower resolution (4 to 5 Å), DEN refinement (Schröder et al., 2007; Schröder et al., 2010) further extends this principle. New refinement methods based on physical energy functions such as Rosetta (DiMaio et al., 2011), are complementary to DEN refinement, and are expected to further improve the accuracy of low-resolution crystal structures. Other recent methods may also be useful at low resolution, including LSSR in Buster (Smart et al., 2008), external structure restraints or jelly body refinement in REFMAC (Murshudov et al., 2011), restraints in torsion angle space based on a reference model (Headd et al., 2012), and normal mode refinement (Kidera and Go, 1992; Delarue, 2008). It should be noted that the principle of achieving higher accuracy of positional information than the diffraction limit is referred to as “super-resolution” in optical microscopy (Moerner, 2007; Pertsinidis et al., 2010). We have therefore suggested adoption of the same term in X-ray crystallography (Schröder et al., 2010).

Here, we explore whether one can obtain more accurate structures than naively suggested by the minimum Bragg spacing of a crystal that diffracts to around 7 Å resolution. This resolution is close to the determinacy point for backbone torsion angles of protein crystal structures, i.e. it is the resolution at which the number of independent Bragg reflections is equal to the number of backbone torsion angles. This relationship (Table S1, W. A. Hendrickson, personal communication) shows that it is reasonable to expect that the secondary structure and tertiary fold of a macromolecule can be determined at around 7 Å resolution. Furthermore, the average X-ray diffraction intensities of a typical macromolecular crystal structure have a characteristic resolution dependence with a local maximum between 6 and 15 Å that is determined by the fold of the molecule; at lower resolution, the intensity distribution is dominated by the envelope of the crystallized molecular entity, and at higher resolution it is determined by the packing of atoms with a maximum at around 5 Å. Thus, the determinacy point for backbone torsion angles is close to the local maximum in X-ray diffraction intensity around 7 Å. The coincidence of high diffraction intensity and determinacy of backbone torsion angles suggests that a reasonable degree of success might be achievable even at such low resolution.

DEN refinement consists of torsion angle refinement interspersed with *B*-factor refinement in the presence of a sparse set of distance restraints that are initially obtained from a reference model (Schröder et al., 2010). Typically, one randomly selected distance restraint is used per atom. The reference model can be simply the starting model for refinement, or it can be a homology or predicted model that provides external information. In this work, the reference model was the search model used for molecular replacement, and only an overall anisotropic *B*-factor refinement was performed as appropriate at very low resolution. During

the process of torsion angle refinement with a slow-cooling simulated annealing scheme, the DEN distance restraints were slowly adjusted in order to fit the diffraction data. The magnitude of this adjustment of the initial distance restraints is controlled by an adjustable parameter,  $\gamma$ . The weight of the DEN distance restraints is controlled by another adjustable parameter,  $w_{\text{DEN}}$ . For the success of DEN refinement it is essential to perform a global search for an optimum parameter pair ( $\gamma$ ,  $w_{\text{DEN}}$ ). Furthermore, for each adjustable parameter pair tested, multiple refinements should be performed with different initial random number seeds for the velocity assignments of the torsion angle molecular dynamics method and different randomly selected DEN distance restraints. The globally optimal model (in terms of minimum  $R_{\text{free}}$ ), possibly augmented by geometric validation criteria, is then used for further analysis. By default, the last two macrocycles of the DEN refinement protocol are performed without any DEN restraints. However, for the low-resolution refinements presented in this paper, the restraints were kept throughout the entire refinement process in keeping with a low ratio of number of observables to number of torsion angle degrees of freedom.

This study was motivated by the recent availability of low-resolution diffraction data of the Photosystem I (PSI) complex collected on a synchrotron light source (the Advanced Light Source, ALS at Lawrence Berkeley National Laboratory, LBL) (Chapman et al., 2011). The synchrotron data were collected on a single crystal and had a limiting resolution of 6 Å, making them comparable to diffraction data obtained at the first hard X-ray FEL light source (the Linac Coherent Light Source, LCLS, at the SLAC National Accelerator Laboratory) with a minimum Bragg spacing of 7.4 Å (limited in resolution by the wavelength of the FEL photons of 6.9 Å used in this study). The availability of a high-resolution ( $d_{\text{min}} = 2.5$  Å) crystal structure of PSI (PDB ID 1jb0) (Jordan et al., 2001) enabled an objective assessment of the accuracy of structures refined by various methods.

Here, we compared DEN refinement of PSI using the ALS diffraction data at 7.4 Å resolution to overall rigid-body refinement, segmented rigid-body refinement, standard refinement consisting of positional minimization, and torsion angle simulated annealing.

We also tested combinations of segmented rigid-body refinement with DEN refinement, and with secondary structure and reference model restrained positional minimization. We assessed the performance of the refinements by (a)  $R_{\text{free}}$ , (b) the root mean square difference (RMSD) to the 2.5 Å resolution crystal structure of PSI, and (c) the significance of features observed in difference maps that were not part of the model used for molecular replacement and refinement. We generated a series of initial models with increasing distance to the 2.5 Å resolution crystal structure, all of which produced a molecular replacement solution. DEN refinement performed better than other methods for all initial models. The most powerful protocol was DEN refinement with initial segmented rigid-body refinement. We also found a good correlation between  $R_{\text{free}}$  and model accuracy among DEN refinements with different adjustable parameters, suggesting that cross-validation is useful even at such low resolution.

## RESULTS

### Molecular replacement with increasingly distant starting models

We generated a series of starting models, designated “M1” to “M6”, in order to assess the sensitivity of molecular replacement phasing and subsequent refinement to the distance between starting and the 2.5 Å resolution crystal structure PSI (PDB ID 1jb0). Model M1 was the 2.5 Å resolution crystal structure of PSI itself. Models M2 through M6 were generated by molecular dynamics starting from M1 to give RMS displacements of Ca backbone atoms from the 2.5 Å resolution crystal structure of PSI that ranged from 2.2 to

4.3 Å. We tested if these models produce the correct solution with molecular replacement phasing using the diffraction data of PSI collected at the ALS (Chapman et al., 2011) (Table 1). The ALS diffraction data were truncated to 7.4 Å resolution to make them comparable the limiting resolution of the first FEL (LCLS) data set of PSI (Chapman et al., 2011). We refer to these truncated data as the 7.4 Å diffraction data of PSI.

For all models, the correct solution emerged as the only solution produced by Phaser (McCoy et al., 2007) (see Experimental Procedures) (Fig. S1). Thus, all models could have been used for molecular replacement against the 7.4 Å diffraction data of PSI, albeit with a non-default parameter for Phaser for model M6 (see Experimental Procedures).

### Overall comparison of refinement methods

The six initial models were subjected to four different refinement methods against the 7.4 Å diffraction data of PSI: (1) overall rigid-body refinement, (2) positional (Cartesian coordinate) minimization, referred to as “standard refinement”, (3) simulated annealing of torsion angles, and (4) DEN refinement as implemented in CNS v1.3 (Schröder et al., 2010). In addition, the most distant model (M6) was also subjected to segmented rigid-body refinement where the PSI protomer was broken up into 12 rigid-body segments that coincided with the 12 protein subunits and associated cofactors. The resulting segment-refined coordinates were further refined with standard refinement, torsion angle refinement, DEN refinement, and “restrained” refinement.

DEN refinement employed the default protocol that is available in CNS v1.3 (Brunger et al., 1998; Schröder et al., 2010) except that only overall anisotropic  $B$ -factor refinement was carried out instead of restrained group  $B$ -factor refinement, and that the DEN restraints were kept throughout the process (see Experimental Procedures for more details). Restrained refinement included both secondary structure and reference model restraints (Headd et al., 2012) as implemented in the program *phenix.refine* (Afonine et al., 2012). We also tried to refine model M6 with the jelly body method implemented in Refmac (Murshudov et al., 2011). However, our attempts did not result in improved  $R_{\text{free}}$ , and the gap between  $R_{\text{free}}$  and  $R$  significantly increased. Since we are uncertain if we used the program optimally for this particular low-resolution crystal structure we refrained from detailed comparisons with Refmac.

The quality and convergence of the refined models was assessed by  $R_{\text{free}}$  (where smaller values are better), C $\alpha$  backbone and chlorophyll  $\text{Mg}^{2+}$  RMSDs to the 2.5 Å resolution crystal structure of PSI (smaller is better), and by  $\langle\sigma\rangle$ , the average Z-score (number of standard deviations above the mean of the difference electron density at the positions of the three omitted iron-sulfur clusters - larger is better). Of course, validation with RMSDs and difference features was only possible because the high-resolution structure of PSI is known.

DEN refinement consistently performed better than any of the other methods tested as assessed by  $R_{\text{free}}$ , RMSD values, and  $\langle\sigma\rangle$  of the iron-sulfur cluster difference map peaks (Fig. S2). The only exception was overall rigid-body refinement starting with model M1 which, by definition, produced RMSD values of zero, whereas the model moved away from M1 upon more extensive refinement, with DEN refinement (refinement statistics in Table 1) producing the smallest deviations (red lines in Fig. S2c,d). The working  $R$  value ( $R_{\text{cryst}}$ ) was quite similar for all refinement methods that go beyond rigid-body refinement (Fig. S2b). In contrast,  $R_{\text{free}}$  showed larger differences between the refined models (Fig. S2a), with DEN refinements always achieving the lowest  $R_{\text{free}}$  values. Thus,  $R_{\text{free}}$  correctly indicated that the DEN refined models are generally the most accurate structures as is reflected in the RMSD values between the refined models and the 2.5 Å resolution crystal structure of PSI (Figs. S2c,d). It should be noted that the relative  $R_{\text{free}}$  ranking of standard refinement and torsion

angle simulated annealing is not well correlated with the RMSD values and  $\langle\sigma\rangle$  of the difference peaks. This discrepancy is related to the vastly different number of refined parameters in standard refinement and torsion angle refinement. Thus,  $R_{\text{free}}$  is most powerful when comparing different models using the same refinement method (see next section).

Since we achieved substantial improvements upon refinement of the most distant initial model (M6) we exclusively focus on refinements starting from this model in the following.

### Relation between $R_{\text{free}}$ and model accuracy

The relationship between  $R_{\text{free}}$  and model accuracy is shown in Figs. 1a,b for structures that were refined with the same DEN refinement protocol, but different adjustable parameters ( $\gamma$ ,  $w_{\text{DEN}}$ ). All refinements started from model M6 and were refined against the 7.4 Å diffraction data of PSI. The  $R_{\text{free}}$  contour plot for the best DEN refinement repeats on a two-dimensional ( $\gamma$ ,  $w_{\text{DEN}}$ ) grid is similar to the corresponding contour plot of the Ca backbone RMSD to the 2.5 Å resolution crystal structure of PSI. In striking contrast, when the “best” refinement repeats were selected by the working  $R$  value ( $R_{\text{cryst}}$ ), the resulting structures were generally much less accurate: in fact, the  $R_{\text{cryst}}$  and RMSD contour plots are approximately anti-correlated (Figs. 1c,d). Thus, cross-validation (including  $R_{\text{free}}$ , but also applicable to other quantities, such as the commonly used measure for model quality,  $\sigma_A$  (Read, 1986)) produces measures that are indicative of the accuracy of the model if the true structure is yet unknown. In contrast, selection of refined models based on  $R_{\text{cryst}}$  can be grossly misleading due to extensive overfitting at low resolution. As shown previously,  $R_{\text{free}}$  is a more objective measure of model quality than  $R_{\text{cryst}}$ . (Brunger, 1992), and the results presented in this paper show that this principle also applies to structures refined at around 7 Å resolution.

### Quality of electron density maps

Electron density maps obtained from the different refinement methods are shown in Fig. 2. All refinements started from model M6 and were refined against the 7.4 Å diffraction data of PSI. Both standard refinement (Fig. 2c) and torsion angle simulated annealing (Fig. 2b) moved away from the 2.5 Å resolution crystal structure of PSI, distorted the  $\alpha$ -helices, and produced fragmented electron density maps; this poor performance correlated with relatively high  $R_{\text{free}}$  values for these refinements. In contrast, DEN refinement generally produced a well-connected electron density map, even for the rightmost  $\alpha$ -helices shown in Fig. 2d, demonstrating that electron density maps obtained by DEN refinement can be superior to those from other refinement methods, as had been demonstrated previously at higher resolution (Schröder et al., 2010; Brunger et al., 2012).

Segmented rigid-body refinement produced fragmented electron density maps that do not indicate how to improve the model (Fig. 2e). Subsequent torsion angle simulated annealing refinement (Fig. 2f) and standard refinement (Fig. 2g) produced more connected electron density maps, but these methods severely distorted the  $\alpha$ -helix geometry, as also indicated by the poor Ramachandran statistics for these refinements (Fig. S3). In contrast, restrained refinement with initial segmented rigid-body refinement maintained good Ramachandran statistics, but it did not correct the right-most  $\alpha$ -helices (Fig. 2h). The optimum method was DEN refinement with initial segmented rigid-body refinement: it generally produced a connected electron density map, even for the rightmost  $\alpha$ -helices, and good  $\alpha$ -helical geometry (Fig. 2i).

### Accuracy of refined structures

The convergence (or divergence) of the various refined structures to the true structure becomes more apparent in the distribution of individual atomic RMSD values from the 2.5 Å resolution crystal structure of PSI (Fig. 3a). The distribution is shifted to smaller values for DEN refinement alone and DEN refinement with initial segmented rigid-body refinement, with a pronounced maximum at 1.2 Å (red solid lines), compared to the models after overall rigid-body refinement or segmented rigid-body refinement (blue lines). Remarkably, the fraction of atoms within 2 Å of the 2.5 Å resolution crystal structure of PSI improves from 12% to 60% for the combination of segmented rigid-body refinement and DEN refinement (Fig. 3b). None of the other tested refinement methods reached this level of accuracy. This shift in the atomic RMSD deviations suggests that structures can be realistically refined beyond rigid-body methods even at around 7 Å resolution. Overall, DEN refinement with initial segmented rigid-body refinement performed best.

### Recovery of larger fragments

DEN refinement, and DEN refinement with initial segmented rigid-body refinement, produced structures that were closer to the 2.5 Å resolution crystal structure of PSI than other tested refinement methods, and produced more significant difference peaks for the three iron-sulfur clusters, which were omitted for validation purposes (Fig. S2e). We next asked the question if it would be possible to recover a larger fragment that was not part of the search model. We performed a series of “omit” refinements against the 7.4 Å diffraction data of PSI with certain  $\alpha$ -helices omitted. A particular example is shown in Fig. 4, demonstrating that the omitted pair of  $\alpha$ -helices (chain F, residues 103–126) is clearly visible in a  $mF_o - DF_c$  difference electron density map when model M1 is refined using DEN (Fig. 4a). When the refinement was started from model M6, using DEN refinement with initial rigid-body refinement, there were significant difference peaks in the regions occupied by the  $\alpha$ -helices although the electron density was somewhat fragmented (Fig. 4b).

## DISCUSSION

Structure determination and refinement at low resolution remains a grand challenge for X-ray crystallography. The availability of high-flux microbeam synchrotron facilities and, potentially, hard X-ray FELs enables application of X-ray crystallography to ever more challenging biological systems. Such systems may not always give well-diffracting crystals, but may nevertheless provide important biological information even at low resolution. The challenge is to obtain an accurate model that makes use of all available information, including external information such as that from high-resolution structures of individual components of the system, as well as use of advanced physics-based energy functions that together make the problem well-determined. In this paper, we have explored the utility of recently developed reciprocal-space refinement methods, in particular DEN refinement (Schröder et al., 2010) and secondary-structure/reference model restrained refinement (Headd et al., 2012). We used an experimental diffraction data set of PSI at 7.4 Å resolution as test case, collected at a synchrotron source (ALS).

We find that DEN refinement improves the accuracy of overall and segmented rigid-body refined models. It is remarkable that DEN refinement alone outperforms segmented rigid-body refinement (Fig. 3b), although it is of course beneficial to precede DEN refinement with segmented rigid-body refinement. In that case, 60% of the atoms were within 2 Å of the 2.5 Å resolution crystal structure of PSI when the refinement was started from the most distant initial model (M6).

Secondary structure and reference model restrained refinement also led to some improvement when used after initial segmented rigid-body refinement (Fig. 3b). However, this improvement was less than that observed for DEN refinement with initial rigid-body refinement. Still, it is interesting that this methodology actually improved the segmented rigid-body refined model in contrast to standard refinement (i.e., without such restraints) that significantly worsened the geometry of the model (Fig. S3). Thus, one would expect that combinations of DEN refinement with secondary structure and reference model restrained refinement could lead to further improvements.

DEN refinement works by guiding the refinement path, increasing the chances of obtaining a better model than with standard refinement, and so the imposition of additional information might make the search for a minimum in  $R_{\text{free}}$  even more efficient. However, the imposition of secondary structure restraints is only advisable if the secondary structural elements are conserved between the initial model and the true structure. In fact, this was not the case for the examples studied here: for example, the rightmost  $\alpha$ -helix shown in Fig. 2 for model M6 has a break that secondary structure restrained refinement cannot overcome (Fig. 2h) whereas DEN refinement moves the two  $\alpha$ -helical fragments together so as to converge to the true structure (Fig. 2i). This particular example is especially interesting since the DEN restraints have no knowledge of the secondary structure of the high-resolution crystal structure of PSI, so the convergence of this  $\alpha$ -helix to the true structure is a consequence of the conformational search that occurs during DEN refinement against the low-resolution diffraction data rather than imposition of some external information. This example is a further demonstration that DEN refinement is a more general method than rigid-body refinement (or, presumably, normal mode refinement) since, at least in principle, it can achieve any type of conformational change. Clearly, there is room for extension of the method by allowing more general coordinate transformations than the relatively simple interpolation scheme currently used in DEN refinement (Schröder et al., 2010).

Our results show that even at low resolution, around 7 Å, the cross-validation  $R$  value ( $R_{\text{free}}$ ) has predictive power: PSI structures that refine to low  $R_{\text{free}}$  values generally have better accuracy than structures with a high  $R_{\text{free}}$ . In contrast, structures that refine to low working  $R$  values ( $R_{\text{crist}}$ ) were further away from the 2.5 Å resolution crystal structure of PSI (Fig. 1). Of course, cross-validation relies on the availability of a sufficient number of reflections that can be omitted for the test set (at least 1,000 reflections are generally advisable (Brunger, 1997)). However, this should not be a problem since most of the systems that will be studied at low resolution comprise large unit cells and hence have a large number of reflections even at low resolution. We also note that the applicability of  $R_{\text{free}}$  to low-resolution structures suggests that the accuracy of several alternate models (e.g., obtained by different sequence alignments during homology modeling) could be tested by refinement of these candidate models using the same refinement protocol.

In summary, we showed that it is possible to refine structures at around 7 Å resolution using DEN refinement or secondary structure/reference model restrained refinement. In both cases, better convergence to true structure was achieved than possible with segmented rigid-body refinement alone (Fig. 3b). For the test case presented here, the optimum protocol is DEN refinement with initial segmented rigid-body refinement.

## EXPERIMENTAL PROCEDURES

### 7.4 Å diffraction data of PSI

Synchrotron diffraction data of PSI single crystals were obtained at beam line 8.2.2 at the ALS as described previously (Chapman et al., 2011); these diffraction data were used in that work for comparison to the diffraction data collected at the LCLS FEL. The synchrotron

diffraction data were collected from a single crystal ( $0.5 \times 1$  mm) of PSI to about 6 Å resolution at 100 K. The data statistics are provided in Table 1. In order to use a limiting resolution comparable to that of the LCLS data of PSI, the synchrotron diffraction data were truncated to 7.4 Å resolution for molecular replacement and refinement. The maximum likelihood estimate of the overall isotropic component of the  $B$ -factor tensor was 66.5 Å<sup>2</sup> for the synchrotron diffraction data, as obtained by the program *phenix.xtriage* (Zwart et al., 2005). The actual overall isotropic component of the  $B$ -factor tensor upon model refinement was 120.9 Å<sup>2</sup>.

### Generation of initial models

Water molecules were removed from the 2.5 Å resolution crystal structure of PSI (PDB ID 1jb0). In addition, the three iron-sulfur clusters were removed from this model for validation purposes. All other cofactors were included (see Table 1 for a list of the cofactors). The resulting model is designated “M1”. This model also serves as the high-resolution comparison model in order to evaluate the performance of the refinements. Five different models were generated by performing simulated annealing molecular dynamics in torsion angle space, using slow-cooling simulated annealing starting at 1,800, 2,200, 2,600, 3,000, and 3,400 K using a cooling rate of 24 fsec per 50 K. These molecular dynamics calculations included crystal symmetry, but the crystallographic diffraction data were not used. We also included randomly selected pair-wise local distance restraints (about 1 per atom, between 3 and 15 Å) to prevent large excursions since molecular dynamics was performed in vacuum at relatively high temperature. The resulting five models are designated “M2”, “M3”, “M4”, “M5”, and “M6”. The resulting  $\text{C}\alpha$  backbone RMSDs to the 2.5 Å resolution crystal structure of PSI were between 2.24 and 4.28 Å.

### Molecular replacement

Molecular replacement phasing using Phaser (McCoy et al., 2007) was performed starting from the six initial models, M1 through M6, with  $B$ -factors transferred from the 1jb0 crystal structure. The 7.4 Å diffraction data of PSI were used (Table 1). Default settings were used for models M1–M5. In each of these cases a unique solution emerged that coincided with the position and orientation of the high-resolution structure of PSI (taking into account different origin choices). In order to obtain a solution for model M6, the rotation function clustering was turned off. A unique solution then emerged, matching 1jb0 crystal structure of PSI. For the subsequent refinements, the  $B$ -factors of the corrected placed and oriented models were set to a uniform value of 50 Å<sup>2</sup>. These models served as starting points for all subsequent refinements, respectively.

### Refinement target functions

The MLF target function (Pannu and Read, 1996) was used for all refinements. Electron density maps were calculated using  $\sigma_A$  weighting. Maximum likelihood target functions were used as implemented in both CNS and *phenix.refine*.

### Overall rigid-body refinement

Overall rigid-body refinement was performed with CNS v1.3 for each of the six starting models. Eight cycles with 20 steps of conjugate gradient minimization (Powell, 1971) were performed.

### Segmented rigid-body refinement

Each of the 12 protein chains and associated cofactors of a PSI protomer were defined as individual rigid bodies. Eight cycles with 100 steps of conjugate gradient minimization (Powell, 1971) were performed with CNS v1.3. The rigid-body refinement method



implemented in *phenix.refine* which uses a L-BFGS optimization method (Nocedal, 1980) produced similar results, however it was necessary to use a single resolution zone, i.e. `rigid_body.number_of_zones` was set to 1. The result of the segmented rigid-body refinement was used as a starting point for DEN refinement, standard refinement, torsion angle simulated annealing refinement, and restrained refinement.

### DEN refinement

The particular initial model was used as both the starting and reference model for DEN refinement (Schröder et al., 2010). For the cases where the initial model was first subjected to segmented rigid-body refinement, the resulting refined model was used as both the starting and reference model for DEN refinement. The refinement protocol was similar to previous work (Schröder et al., 2010) (as also described in the tutorial for DEN refinement in CNS v1.3, <http://cns-online.org/v1.3/>) except that only overall anisotropic *B*-factor refinement was carried out instead of restrained group *B*-factor refinement, and that the DEN restraints were kept throughout the process. In the default protocol, the DEN restraints are turned off during the last two macrocycles. Specifically, eight macrocycles of torsion angle refinement with a slow-cooling simulated annealing scheme were performed where the first cycle always used  $\gamma = 0$ , the following seven cycles used a specified value for  $\gamma$  (see below).

DEN distance restraints were generated from *N* randomly selected pairs of atoms in the reference model that were separated by 3 to 15 Å in space; no sequence selection criterion was used. Therefore, distances were drawn from any pair of atoms between any protein chain and cofactor. The value of *N* was chosen to be equal to the number of atoms, so the set of distance restraints was relatively sparse with an average of one restraint per atom. The minimum of the initial DEN potential was set to the coordinates of the particular starting model. We determined the optimum values of the  $\gamma$  and  $w_{DEN}$  parameters of DEN refinement by a global two-dimensional grid search. At each grid point, twenty refinement repeats were performed with different random initial velocities and different randomly selected DEN distances. We used thirty combinations of six  $\gamma$  values [0.0, 0.2, 0.4, 0.6, 0.8, 1.0] and five  $w_{DEN}$  values [3, 10, 30, 100, 300]. In addition, six different temperatures for the slow-cooling simulated annealing scheme were tested [300, 600, 1000, 1500, 2000, and 3000 K] except for the cases of DEN refinement with initial segmented rigid-body refinement where only 3000 K was used. A representative example of the results of the grid search is shown in Fig. 2a. The SBGrid DEN refinement portal ([www.sbgrid.org](http://www.sbgrid.org)) was used for most of these refinements. Out of all these resulting models, the one with the lowest  $R_{free}$  value was used for subsequent analysis.

### Torsion angle simulated annealing

As a control, we performed twenty repeats with  $w_{DEN} = 0$  at 3000 K. This corresponded to using the refinement protocol without DEN restraints, with results being independent of  $\gamma$ . Out of the resulting models, the one with the lowest  $R_{free}$  value was used for subsequent analysis.

### Standard refinement

As a further control, eight macrocycles of 200 steps of conjugate gradient minimization using the L-BFGS optimizer implemented in CNS v1.3 were performed starting from the same models that were used for the DEN refinements. These refinements did not employ DEN restraints.

## Secondary structure and reference restrained refinement

As an additional control, we performed secondary structure and reference model (Headd et al., 2012) restrained refinement with *phenix.refine* (Afonine et al., 2012). A simulated annealing refinement scheme was used with default control parameters except that a single group *B*-factor was refined for the entire model and no individual atomic displacement parameters were refined, and a starting temperature of 5000 K was used for the simulated annealing stage. Additionally, secondary structure restraints (Headd et al., 2012) were automatically determined from the starting model and applied during refinement. Reference model restraints (Headd et al., 2012) were generated from the starting model and used to restrain the model during refinement. A total of three macrocycles of refinement were performed with simulated annealing performed only in the second macrocycle. The weight on the X-ray term in the refinement (*wxc\_scale*) was reduced by a factor of two, i.e. the weight was 0.25. Geometric restraints for the ligands in the structure were generated using *phenix.elbow* (Moriarty et al., 2009). Manual modifications were made to the chlorophyll restraints to maintain a planar porphyrin ring geometry.

## Assessment of the quality and accuracy of the refined models

The various refinement methods were assessed by three criteria:  $R_{\text{free}}$ , RMSD to the 2.5 Å resolution crystal structure of PSI (PDB ID 1j0), and the significance of the difference peaks for the three iron-sulfur clusters that were omitted in the refinement. The  $R_{\text{free}}$  value was used to provide a model-free assessment of the quality of the refined model. The refined models were compared to the 2.5 Å resolution crystal structure of PSI by computing the RMSD for all C $\alpha$  backbone atoms and the RMSD for the Mg<sup>2+</sup> ions of the 96 chlorophyll cofactors; prior to computing the RMSD, the models were least-squares superimposed using the backbone C $\alpha$  atoms to account for possible translation of the model in the z-direction since space group P6<sub>3</sub> has an arbitrary origin choice in the z-direction. For each refined model,  $mF_o - DF_c$  difference maps were computed. For each of the three iron-sulfur clusters,  $\sigma$ , the Z-score (standard deviation above the mean) of the difference electron density was determined and the average of the three  $\sigma$  values calculated as  $\langle \sigma \rangle$ . Since in some cases, the refinements had moved some of the sidechains of the four coordinating cysteine residues into the difference density, the CB and SG atoms of these residues were excluded in the calculation of the phases for the difference electron density maps. For the better performing refinements, clear peaks emerged in the difference density maps within the extent of the iron-sulfur clusters; the  $\sigma$  values at these peak positions were used. For some of the poorer performing refinements, no clear peak in the difference density map was found within the extent of an iron-sulfur cluster. In these cases, the significance of the corresponding difference density was estimated by the value of the difference electron density map at the center of the cluster. These procedures were uniformly applied to all refinements.

## Computer programs used

MOSFLM (Leslie, 2006) was used for the indexing and integration of the ALS data of PSI. The analysis of diffraction data was performed with the *phenix.xtriage* program (Zwart et al., 2005). The Crystallography and NMR System (CNS) (Brunger et al., 1998) v1.3 was used for DEN refinement, standard (positional minimization) refinement, and torsion angle simulated annealing refinement. *phenix.refine* was used for secondary structure and reference model restrained refinement (Adams et al., 2010; Afonine et al., 2012). PyMOL (DeLano, 2002) was used for molecular illustrations, structure, and electron density map superposition. Molprobit (Chen et al., 2010) was used to calculate the Ramachandran statistics.

## Supplementary Material

Refer to Web version on PubMed Central for supplementary material.

## Acknowledgments

We thank Thomas White and Henry Chapman for stimulating discussions and critical reading of the manuscript, and Corie Ralston for support at beamline 8.2.2 at ALS. ATB acknowledges support by HHMI, ML is supported by award GM063817 from NIH, PDA acknowledges support by the US Department of Energy under contract No. DE-AC03-76SF00098 and NIH/NIGMS grant No. P01GM063210, and RF and PF acknowledge support by the Center for Bio-Inspired Solar Fuel Production, an Energy Frontier Research Center funded by the Department of Energy (DOE), Office of Basic Energy Sciences (award DE-SC0001016). Experiments were carried out the Advanced Light Source, a National User Facilities operated respectively by Stanford University and the University of California on behalf of the DOE, Office of Basic Energy Sciences. ATB and PDA performed calculations, analyzed the results, and wrote the paper. RF measured and processed the data at beam line 8.2.2 at ALS. GFS, ML, PF, and RF analyzed the results and wrote the paper.

## References

- Adams PD, Afonine PV, Bunkoczi G, Chen VB, Davis IW, Echols N, Headd JJ, Hung LW, Kapral GJ, Grosse-Kunstleve RW, et al. PHENIX: a comprehensive Python-based system for macromolecular structure solution. *Acta Crystallogr D Biol Crystallogr*. 2010; 66:213–221. [PubMed: 20124702]
- Afonine PV, Grosse Kunstleve RW, Echols N, Headd JJ, Moriarty NW, Mustyakimov M, Terwilliger TC, Urzhumtsev A, Zwart PH, Adams PD. Towards automated crystallographic structure refinement with phenix.refine. *Acta Cryst*. 2012; D68:352–367.
- Brunger AT. Free R value: a novel statistical quantity for assessing the accuracy of crystal structures. *Nature*. 1992; 355:472–475. [PubMed: 18481394]
- Brunger AT. Free R value: cross-validation in crystallography. *Methods Enzymol*. 1997; 277:366–396. [PubMed: 18488318]
- Brunger AT, Adams PD, Clore GM, DeLano WL, Gros P, Grosse-Kunstleve RW, Jiang JS, Kuszewski J, Nilges M, Pannu NS, et al. Crystallography & NMR system: A new software suite for macromolecular structure determination. *Acta Crystallogr D Biol Crystallogr*. 1998; 54:905–921. [PubMed: 9757107]
- Brunger AT, Das D, Deacon AM, Grant J, Terwilliger TC, Read RJ, Adams PD, Levitt M, Schroder GF. Application Of DEN-Refinement And Automated Model-Building To A Difficult Case Of Molecular Replacement Phasing: The Structure Of A Putative Succinyl-Diaminopimelate Desuccinylase From *Corynebacterium Glutamicum*. *Acta Cryst D*. 2012; 68:391–403. [PubMed: 22505259]
- Chapman HN, Fromme P, Barty A, White TA, Kirian RA, Aquila A, Hunter MS, Schulz J, DePonte DP, Weierstall U, et al. Femtosecond X-ray protein nanocrystallography. *Nature*. 2011; 470:73–77. [PubMed: 21293373]
- Chen VB, Arendall WB 3rd, Headd JJ, Keedy DA, Immormino RM, Kapral GJ, Murray LW, Richardson JS, Richardson DC. MolProbity: all-atom structure validation for macromolecular crystallography. *Acta Crystallogr D Biol Crystallogr*. 2010; 66:12–21. [PubMed: 20057044]
- DeLano, WL. The Pymol Molecular Graphics System on World Wide Web. 2002. <http://www.pymol.org>
- Delarue M. Dealing with structural variability in molecular replacement and crystallographic refinement through normal-mode analysis. *Acta Crystallogr D Biol Crystallogr*. 2008; 64:40–48. [PubMed: 18094466]
- Diederichs K, Karplus PA. Improved R-factors for diffraction data analysis in macromolecular crystallography. *Nat Struct Biol*. 1997; 4:269–275. [PubMed: 9095194]
- DiMaio F, Terwilliger TC, Read RJ, Wlodawer A, Oberdorfer G, Wagner U, Valkov E, Alon A, Fass D, Axelrod HL, et al. Improved molecular replacement by density- and energy-guided protein structure optimization. *Nature*. 2011; 473:540–543. [PubMed: 21532589]

- Headd JJ, Echols N, Afonine PV, Grosse Kunstleve RW, Chen VB, Moriarty NW, Richardson DC, Richardson JS, Adams PD. Knowledge-based restraints in phenix.refine for improved macromolecular refinement at low resolution. *Acta Cryst D*. 2012 in press.
- Jordan P, Fromme P, Witt HT, Klukas O, Saenger W, Krauss N. Three-dimensional structure of cyanobacterial photosystem I at 2.5 Å resolution. *Nature*. 2001; 411:909–917. [PubMed: 11418848]
- Kidera A, Go N. Normal mode refinement: crystallographic refinement of protein dynamic structure. I. Theory and test by simulated diffraction data. *Journal of molecular biology*. 1992; 225:457–475. [PubMed: 1593630]
- Leslie AGW. The integration of macromolecular diffraction data. *Acta Crystallogr D*. 2006; 62:48–57. [PubMed: 16369093]
- McCoy AJ, Grosse-Kunstleve RW, Adams PD, Winn MD, Storoni LC, Read RJ. Phaser crystallographic software. *J Appl Crystallogr*. 2007; 40:658–674. [PubMed: 19461840]
- Moerner WE. New directions in single-molecule imaging and analysis. *Proc Natl Acad Sci U S A*. 2007; 104:12596–12602. [PubMed: 17664434]
- Moriarty NW, Grosse-Kunstleve RW, Adams PD. electronic Ligand Builder and Optimization Workbench (eLBOW): a tool for ligand coordinate and restraint generation. *Acta Crystallogr D Biol Crystallogr*. 2009; 65:1074–1080. [PubMed: 19770504]
- Murshudov GN, Skubak P, Lebedev AA, Pannu NS, Steiner RA, Nicholls RA, Winn MD, Long F, Vagin AA. REFMAC5 for the refinement of macromolecular crystal structures. *Acta Crystallogr D Biol Crystallogr*. 2011; 67:355–367. [PubMed: 21460454]
- Nocedal J. Updating quasi-newton matrices with limited storage. *Mathematics of Computation*. 1980; 35:773–782.
- Pannu NS, Read RJ. Improved structure refinement through maximum likelihood. *Acta Crystallogr A*. 1996; 52:659–668.
- Pertsinidis A, Zhang Y, Chu S. Localization, registration and distance measurements between single-molecule fluorescent probes with sub-nanometer precision and accuracy. *Nature*. 2010 submitted.
- Powell MJD. On the convergence of a variable metric algorithm. *J Inst Math Applic*. 1971; 7:21–36.
- Read RJ. Improved Fourier Coefficients for Maps Using Phases from Partial Structures with Errors. *Acta Crystallogr A*. 1986; 42:140–149.
- Sanishvili R, Nagarajan V, Yoder D, Becker M, Xu S, Corcoran S, Akey DL, Smith JL, Fischetti RF. A 7 microm mini-beam improves diffraction data from small or imperfect crystals of macromolecules. *Acta Crystallogr D Biol Crystallogr*. 2008; 64:425–435. [PubMed: 18391409]
- Schröder GF, Brunger AT, Levitt M. Combining efficient conformational sampling with a deformable elastic network model facilitates structure refinement at low resolution. *Structure*. 2007; 15:1630–1641. [PubMed: 18073112]
- Schröder GF, Levitt M, Brunger AT. Super-resolution biomolecular crystallography with low-resolution data. *Nature*. 2010; 464:1218–1222. [PubMed: 20376006]
- Smart, O.; Brandl, M.; Flensburg, C.; Keller, P.; Paciorek, W.; Vonrhein, C.; Womack, T.; Bricogne, G. Refinement with Local Structure Similarity Restraints (LSSR) enables exploitation of information from related structures and facilitates use of NCS. *Abstr Annu Meet Am Crystallogr Assoc*; Knoxville, TN. 2008.
- Zwart PH, Grosse Kunstleve RW, Adams PD. Characterization of X-ray data sets. *CCP4 Newsletter*. 2005:42.

**HIGHLIGHTS**

- Improved models by DEN refinement at 7 Å
- Best method is DEN refinement with initial segmented rigid-body refinement
- $R_{\text{free}}$  has predictive power at 7 Å

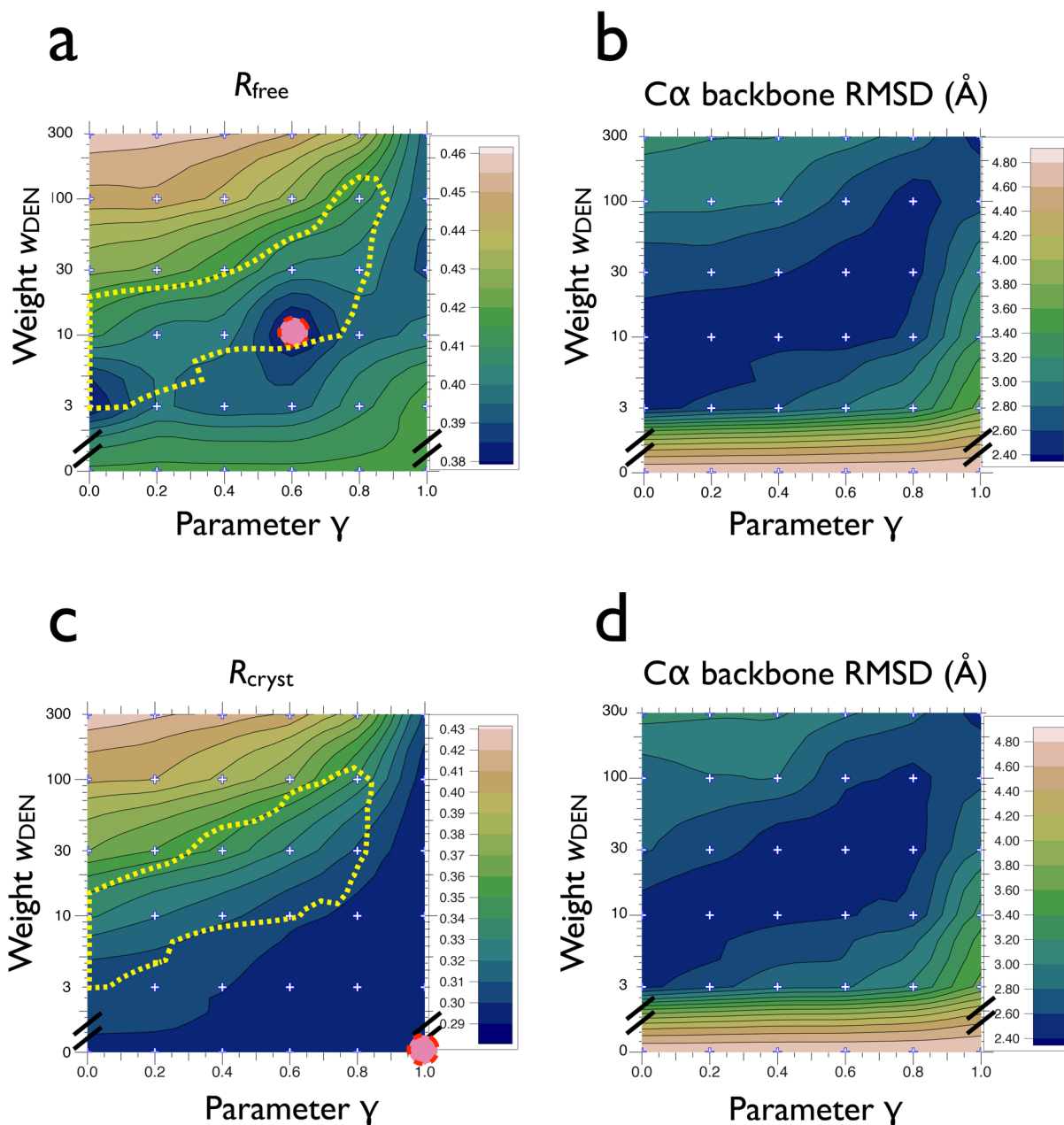


**Figure 1.**

$R_{\text{free}}$  and corresponding RMSD to the 2.5  $\text{\AA}$  structure of PSI (PDB ID 1jb0) for DEN refinements that were performed against the 7.4  $\text{\AA}$  diffraction data of PSI, starting from model M6 with initial segmented rigid-body refinement (denoted “M6+seg” in Fig. S2). Panel (a) shows the lowest  $R_{\text{free}}$  value for each parameter pair ( $\gamma$ ,  $w_{\text{DEN}}$ ) among 20 repeats; for each parameter pair we performed 20 repeats of the DEN refinement protocol described in Experimental Procedures. The temperature of the slow-cooling simulated annealing scheme was 3000 K. The  $R_{\text{free}}$  value is contoured using values calculated on a  $6 \times 6$  grid (marked by small ‘+’ signs) where the parameter  $\gamma$  was [0.0, 0.2, 0.4, 0.6, 0.8, 1.0] and  $w_{\text{DEN}}$  was [0, 3, 10, 30, 100, 300]; the results for  $w_{\text{DEN}} = 0$  (i.e., torsion angle refinement without DEN restraints) are independent of  $\gamma$ , so the same value was used for all grid points

with  $w_{\text{DEN}} = 0$ . The contour plot shows minima in the range  $30 \leq w_{\text{DEN}} \leq 3$ ; the absolute minimum is at  $w_{\text{DEN}} = 10$ ,  $\gamma = 0.6$  (dashed circle), corresponding to an  $R_{\text{free}}$  value of 0.38. In contrast, the lowest  $R_{\text{free}}$  value for refinement without DEN restraints ( $w_{\text{DEN}} = 0$ ) is only 0.42. The yellow dashed line indicates the region of DEN-refined models with the smallest C $\alpha$  backbone RMSD to the 2.5 Å structure of PSI. Panel (b) shows the C $\alpha$  backbone RMSD between the refinement repeat that produced the lowest  $R_{\text{free}}$  value and the 2.5 Å structure of PSI for each of the parameter pairs ( $\gamma$ ,  $w_{\text{DEN}}$ ). Note the large RMSD for refinements without DEN restraints ( $w_{\text{DEN}} = 0$ ). Panel (c) shows the lowest  $R_{\text{cryst}}$  value for each of the parameter pairs ( $\gamma$ ,  $w_{\text{DEN}}$ ) among 20 repeats; the absolute minimum is at  $w_{\text{DEN}} = 0$ ,  $\gamma = 1$  (dashed circle). The yellow dashed line indicates the region of DEN-refined models with the smallest C $\alpha$  backbone RMSD to the 2.5 Å structure of PSI. Panel (d) shows the C $\alpha$  backbone RMSD between the refinement repeat that produced the lowest  $R_{\text{cryst}}$  value and the 2.5 Å structure of PSI for each of the parameter pairs ( $\gamma$ ,  $w_{\text{DEN}}$ ).  $R_{\text{cryst}}$  and the C $\alpha$  backbone RMSD are approximately anti-correlated. See also Figure S1 and Table S1.

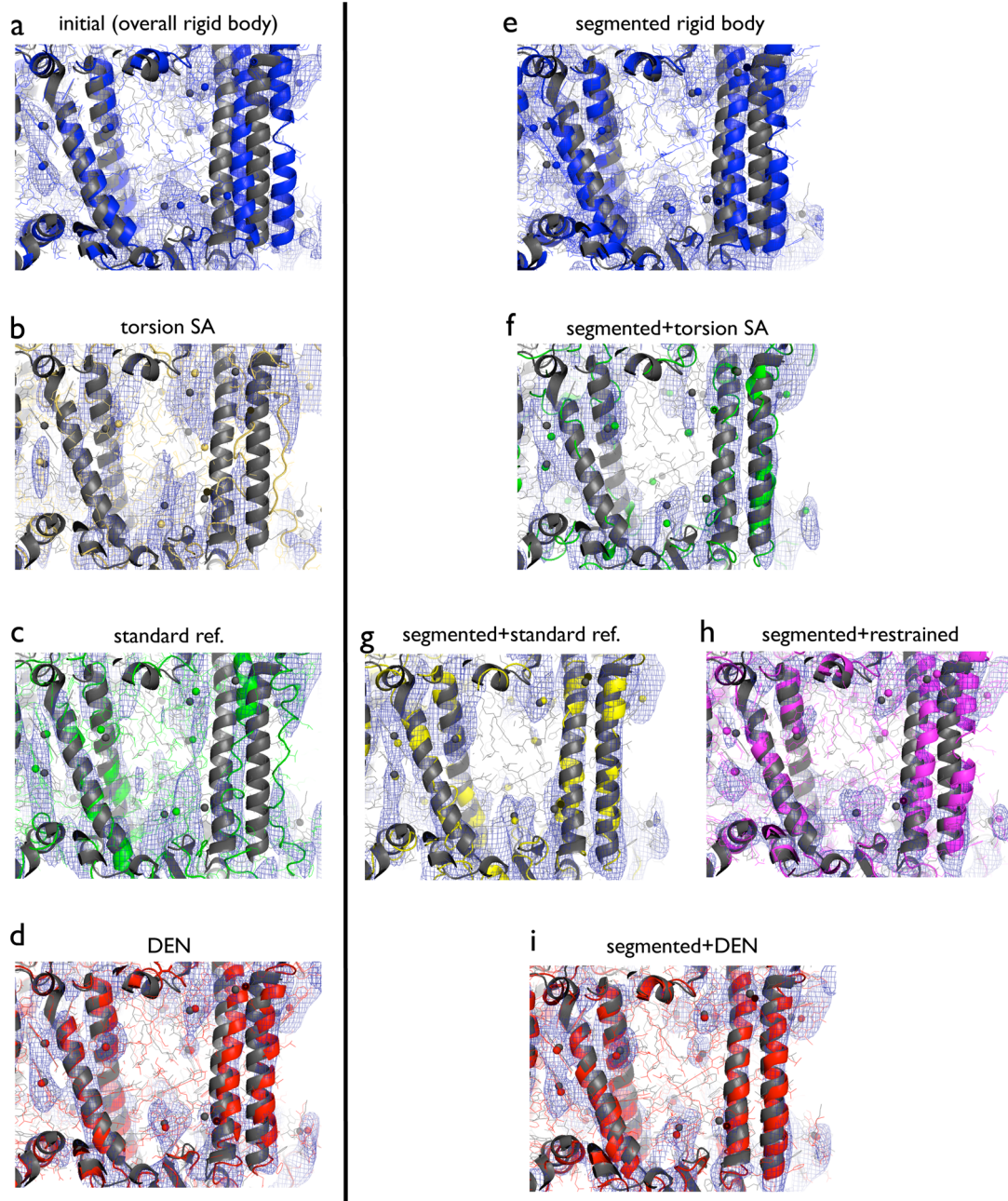


**Figure 2.**

Models and corresponding  $m2F_o-DF_c$  electron density maps for specified refinements against the 7.4 Å diffraction data of PSI, starting from model M6. The electron density maps (blue mesh) were calculated with phases from the corresponding refined model and contoured at  $1.5\sigma$ . The 2.5 Å structure of PSI (PDB ID 1jb0) is shown in dark gray in each of the panels. Spheres indicate  $Mg^{2+}$  ions at the center of the chlorin rings. All non-hydrogen atoms are shown (lines) along with a cartoon representation. The region shown in the figure includes four  $\alpha$ -helices (residues 54–100, 155–181, 669–694, and 720–750 of chain A) along with their protein environment and associated co-factors. (a) Initial, overall rigid-body refined model (blue). (b) Model obtained by torsion angle simulated annealing



(yellow). **(c)** Model obtained by standard refinement (green). **(d)** Model obtained by DEN refinement (red). **(e)** Model obtained by segmented rigid-body refinement (blue). **(f)** Model obtained by torsion angle simulated annealing with initial segmented rigid-body refinement (green). **(g)** Model obtained by standard refinement with initial segmented rigid-body refinement (yellow). **(h)** Model obtained by refinement with secondary structure and reference restraints with *phenix.refine* with initial segmented rigid-body refinement (magenta). **(i)** Model obtained by DEN refinement with initial segmented rigid-body refinement (red). Refinement protocols are described in Experimental Procedures. See also Figure S2.

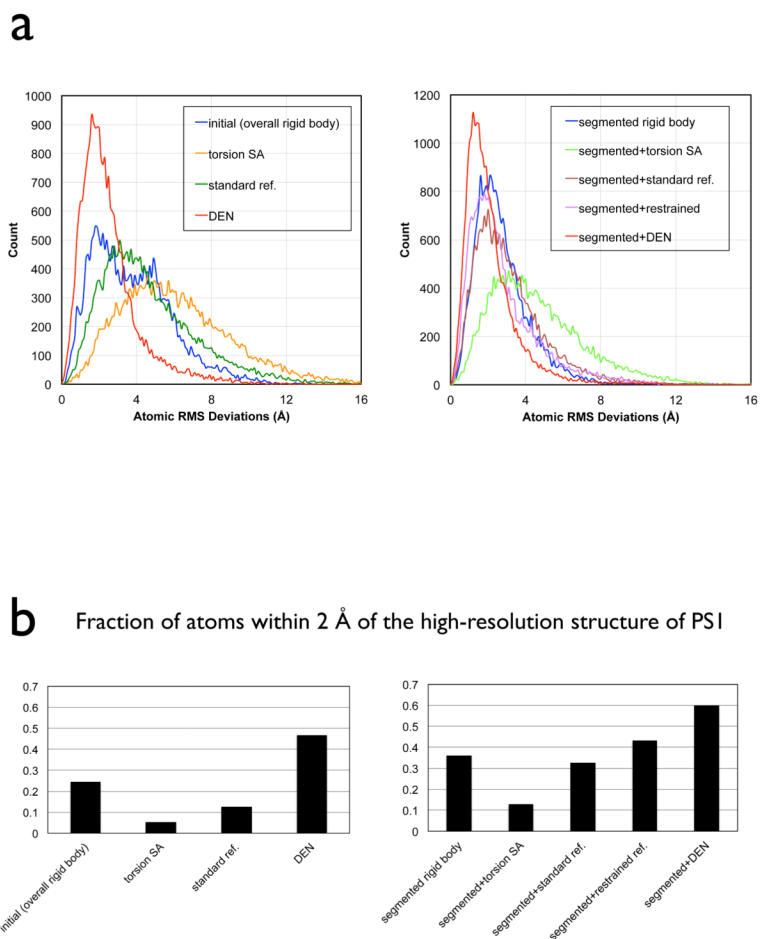


**Figure 3.** Individual atomic RMS deviations to the 2.5 Å structure of PSI (PDB ID 1jb0) for specified refinements against the 7.4 Å diffraction data of PSI, starting from the model M6. **(a)** Histogram of individual atomic RMS deviations between the model refined by the specified method and the 2.5 Å structure of PSI. **(b)** Fraction of atoms that show RMS deviations less than 2 Å from the 2.5 Å structure of PSI. See also Figure S3.

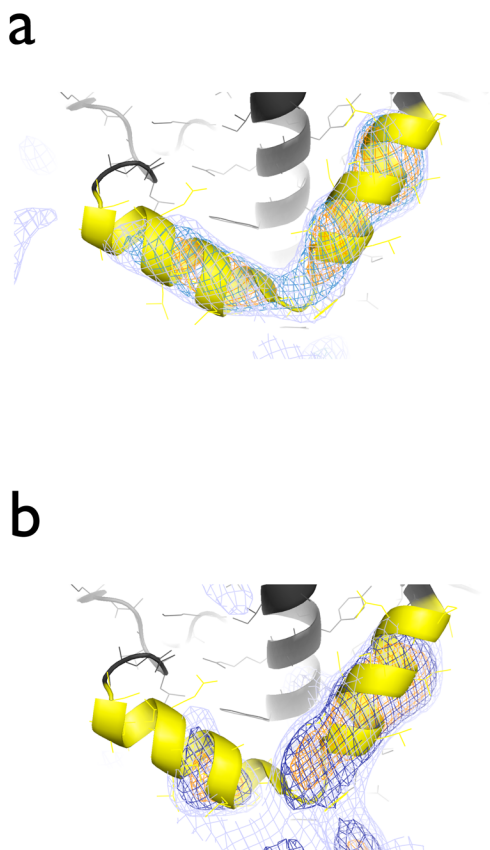


**Figure 4.**

(a) Omit DEN refinement against the 7.4 Å diffraction data of PSI. The initial model was model M1, i.e., the 2.5 Å structure of PSI (PDB ID 1jb0), with a pair of  $\alpha$ -helices omitted (chain F, residues 103:126). Shown are  $mF_o-DF_c$  electron density maps at 3  $\sigma$  (orange), 2.5  $\sigma$  (blue), and 2  $\sigma$  (light blue). Note that these two  $\alpha$ -helices are located at the detergent-exposed periphery of the PSI complex. (b) DEN refinement with initial segmented rigid body refinement starting from model M6, with the same  $\alpha$ -helix pair omitted, against the 7.4 Å diffraction data of PSI. Shown are  $mF_o-DF_c$  electron density maps at 3  $\sigma$  (orange), 2.5  $\sigma$  (blue), and 2  $\sigma$  (light blue).

Table 1

## Data and refinement statistics

Space group	P6 <sub>3</sub>		
Unit cell parameters	a = 283.70 Å, b = 283.70 Å, c = 165.29 Å		
<b>Data collection</b>			
Wavelength (Å)	1.00		
Resolution range (Å)	65.2–6.0		
Number of observations	110202		
Number of unique reflections	18989		
Completeness (%)	99.3 (100) <sup>a</sup>		
Mean <i>I</i> σ( <i>I</i> )	3.5 (2.9) <sup>a</sup>		
<i>R</i> <sub>merge</sub> on <i>I</i> (%) <sup>b</sup>	44.7 (51.3) <sup>a</sup>		
<i>R</i> <sub>meas</sub> on <i>I</i> (%) <sup>c</sup>	49.4 (55.9) <sup>a</sup>		
Highest resolution shell (Å)	6.32–6.00		
<b>Model and refinement statistics for DEN refinement, starting with model M1</b>			
Resolution range (Å)	49–7.4		
No. of reflections (total)	10004	Cutoff criteria	F >0
No. of reflections (test)	508	<i>R</i> <sub>cryst</sub>	0.260 <sup>d</sup>
Completeness (%)	99.5	<i>R</i> <sub>free</sub>	0.291 <sup>d</sup>
Ramachandran (% favored)	79		
Ramachandran (% outliers)	10.7		
<b>Stereochemical parameters</b>			
Bond angle RMSD (°)	1.29		
Bond length RMSD (Å)	0.008		
Average protein isotropic <i>B</i> -factor (Å <sup>2</sup> )	120.9		
Protein	12 chains with a total of 2334 residues		
Chlorophyll	96 (95 Chlorophyll a, 1 Chlorophyll a')		
Beta-carotene	21		
Phylloquinone	2		
1,2-dipalmitoyl-phosphatidyl-glycerole	3		
1,2-distearoyl-monogalactosyl-diglyceride	1		
Ca <sup>2+</sup>	1		
FeS	3 <sup>e</sup>		

<sup>a</sup>Highest resolution shell.

<sup>b</sup> $R_{\text{merge}} = \frac{\sum_{\text{hkl}} \sum_i |I_i(\text{hkl}) - \langle I(\text{hkl}) \rangle|}{\sum_{\text{hkl}} \sum_i I_i(\text{hkl})}$ .

<sup>c</sup> $R_{\text{meas}}$  (redundancy-independent  $R_{\text{merge}}$ ) =  $\frac{\sum_{\text{hkl}} [n/(n-1)]^{1/2} \sum_j |f_j(\text{hkl}) - \langle f(\text{hkl}) \rangle|}{\sum_{\text{hkl}} \sum_j f_j(\text{hkl})}$  (Diederichs and Karplus, 1997).

$d_{R=\Sigma} = \sum (|F_{\text{obs}}| - |F_{\text{calc}}|) / \sum |F_{\text{obs}}|$  where  $F_{\text{calc}}$  and  $F_{\text{obs}}$  are the calculated and observed structure factor amplitudes, respectively.  $R_{\text{free}}$  as for  $R$ , but for 5% of the total reflections chosen at random and omitted from refinement.  $R_{\text{cryst}}$  as for  $R$ , but for the remaining 95% of the reflections.

<sup>e</sup>Omitted in refined model for validation purposes.